Nat. Hazards Earth Syst. Sci. Discuss., 3, 3225–3250, 2015
www.nat-hazards-earth-syst-sci-discuss.net/3/3225/2015/
doi:10.5194/nhessd-3-3225-2015

Natural Hazards and Earth System Sciences
Discussions
Open Access

Spatial analysis of damaged vegetation in the Mianyuan River basin after the Wenchuan Earthquake

H. Z. Zhang[1,2,3], J. R. Fan[2], X. M. Wang[1,3], T. H. Chi[1], and L. Peng[1]

[1]Institute of Remote Sensing and Digital Earth, Chines Academy of Sciences, Beijing, 100101, China
[2]Institute of Mountain Hazards and Environment, Chines Academy of Sciences, Chengdu, 610041, China
[3]University of Chinese Academy of Sciences, Chinese Academy of Sciences, Beijing, 100049, China

Received: 3 April 2015 – Accepted: 19 April 2015 – Published: 11 May 2015

Correspondence to: H. Z. Zhang (zhanghz@radi.ac.cn) and L. Peng (pl20158@126.com)

Published by Copernicus Publications on behalf of the European Geosciences Union.

Abstract

The 2008 Wenchuan earthquake destroyed large areas of vegetation. Presently, these areas of damaged vegetation are at various stages of recovery. In this study, we present a probabilistic approach for slope stability analysis that quantitatively relates data on earthquake-damaged vegetation with slope stability in a given river basin. The Mianyuan River basin was selected for model development, and earthquake-damaged vegetation and post-earthquake recovery conditions were identified via the normalized difference vegetation index (NDVI), from multi-temporal (2001–2014) remote sensing images. DSAL (digital elevation model, slope, aspect, and lithology) spatial zonation was applied to characterize the survival environments of vegetation, which were used to discern the relationships between successful vegetation regrowth and environmental conditions. Finally, the slope stability susceptibility model was trained through multivariate analysis of earthquake-damaged vegetation and its controlling factors (i.e. topographic environments and material properties). Application to the Subao River basin validated the proposed model, showing that most of the damaged vegetation areas have high susceptibility levels (88.1 % > susceptibility level 3, and 61.5 % > level 4). Our modelling approach may also be valuable for use in other regions prone to landslide hazards.

1 Introduction

On 12 May 2008, the high-magnitude (Ms 8.0) Wenchuan earthquake struck China, and the large release of energy triggered many geo-hazards at different scales; catastrophic landslides and collapses were particularly widespread in middle- and high-elevation mountainous areas (Cui et al., 2009; Huang and Li, 2009a). These geo-hazards resulted in massive movements of surface material that led to large areas of damaged vegetation, and in some places the vegetation was completely destroyed (Cui et al., 2012). Presently, the areas of damaged vegetation are at various stages

NHESSD
3, 3225–3250, 2015

of recovery and some have fully recovered within only a few years of the earthquake (Liu et al., 2010). Nevertheless, the potential for future slope instability still exists in this region (Khan et al., 2013). Few studies have focused explicitly on the recovery process of earthquake-damaged vegetation in this region. For example, Zhang et al. (2014) documented the natural recovery of forests after the earthquake and revealed that factors including soil cover and slope were correlated with successful vegetation recovery (Zhang et al., 2014). Soil moisture is one of the most important environmental factors for vegetation recovery in the landslide sites (Lin et al., 2005).

The occurrence and frequency of landslides in an area depend fundamentally on the interaction between triggering mechanisms and natural conditions (Lee et al., 2008; Guzzetti et al., 2012; Peruccacci et al., 2012; Borgomeo et al., 2014). Events such as the Wenchuan earthquake not only trigger serious co-seismic landslides, but can also lead to increased long-term post-seismic slope instability (Koi et al., 2008; Tang et al., 2011). We consider that the locations of vegetation damage are related to slope stability, and that recovery conditions can represent its suffered landslides. Establishing statistical relationships between damaged vegetation and the environmental conditions under which vegetation will recover, hereafter called the "survival environment," is an important task for predicting and mapping areas susceptible to future slope failure.

This paper presents a general framework for determining the relationships between landslide-damaged vegetation and the topographical and vegetative factors associated with survival environments. The Mianyuan River basin was selected for model development, and we identified earthquake-damaged vegetation and post-earthquake recovery conditions using the normalized difference vegetation index (NDVI) from multi-temporal (2001–2014) remote sensing images. We then applied DSAL (digital elevation model, slope, aspect, and lithology) spatial zonation to characterize the survival environments of vegetation, which were used to discern the relationships between environmental conditions and successful vegetation regrowth. Finally, the slope susceptibility model was trained through multivariate analysis of earthquake-damaged vegetation and its controlling factors (i.e. topographic environments and material properties). The

NHESSD
3, 3225–3250, 2015

proposed model was then applied to the Subao River basin to evaluate whether or not the data could be used to assess future susceptibility to slope failure in regions affected by the Wenchuan earthquake. In addition, the recovery capacity model of the damaged vegetation was trained through multivariate analysis of recovery vegetation and its survival factors (i.e. topographic environments and material properties), and was used to assess the landslide processes of the damaged vegetation areas under certain conditions.

2 The study area

2.1 The study area location

The study area is located in the upstream reaches of the Mianyuan River watershed (31°26′–31°42′ N, 103°54′–104°11′ E), in Mianzhu County, Sichuan Province, China, and is approximately 100 km north of Chengdu, the provincial capital. Most importantly, the 2008 Wenchuan earthquake generated high levels of ground shaking (seismic intensity X) in Mianyuan River basin (Fig. 1a). The watershed ranges from 669 to 4417 m in elevation and has an area of approximately 411 km^2 (Fig. 1b).

The Mianyuan River is situated in the transitional mountainous belt between the Sichuan basin and the western Sichuan Plateau, which is characterized by rugged mountains with deeply incised valleys. Active geotectonic movements induced by the complicated fault system occur frequently in this region. The Longmenshan thrust belt, which ruptured during the 2008 Wenchuan earthquake, runs through the central part of the Mianyuan River basin (Fig. 1c). The rocks of Mianyuan River basin primarily consist of Sinian sandstone and siltstone (Z); Cambrian sandstone, siltstone, and slate (E); Silurian phyllite, schist, and slate (S); Devonian dolomite limestone and sandstone (D); Carboniferous limestone (C); Permian limestone and shale (P); Triassic sandstone, dolomite, limestone, siltstone, and shale (T); Quaternary deposits (Q); and magmatic

NHESSD
3, 3225–3250, 2015

rocks, granite, and diorite (r). These lithologies are based on 1 : 200 000 scale geological maps.

2.2 Pre- and post-earthquake vegetation in Mianyuan River Basin

The basin is influenced by a subtropical moist climate and monsoonal rains that start in early June and continue until September. Mean annual precipitation is approximately 1500–1700 mm, of which about 70 % is monsoonal; mean annual temperature is 15.7 °C (http://www.mz.gov.cn). As a result of this variable climate, the basin was rich in vegetation before the Wenchuan earthquake (Fig. 2a and b).

During the Wenchuan earthquake, the earthquake-induced geo-hazards resulted in massive movement of surface material that diminished and destroyed large areas of vegetation (Fig. 2c and d). These damaged vegetation areas alter the spectral signatures and NDVI values recorded on remote sensing images. These data sets are derived from both the red and near-infrared spectral bands and are sensitive to changes in biophysical conditions of vegetation, and can therefore be used to detect these damaged areas. Following the earthquake, obvious changes in NDVI values indicated areas (Fig. 2e and f) of damaged vegetation (Liu et al., 2012), which were distributed along the stream network of the basin (Fig. 2g). Statistical analysis shows that the total size of the damaged area was about 95.4 km^2, which accounts for 23.2 % of the area of Mianyuan River basin.

More recently, 17 June 2014 Landsat-8 images (Fig. 2h) of the basin indicate that most areas of damaged vegetation have recovered, whereas other areas have not. To analyse this recovery process in detail, the 17 June 2014 NDVI image was processed to extract the unrecovered vegetation areas. The earthquake-damaged and recovered vegetation areas are shown in Fig. 2i. The results indicate that these areas of damaged vegetation exhibit various stages of recovery depending on their environments (particularly local topographical conditions). Statistical analysis shows that approximately 57.5 km^2 (60.3 %) of the total damaged vegetation area has recovered.

NHESSD
3, 3225–3250, 2015

3 Assessment of slope stability susceptibility

3.1 Spatial analysis earthquake-damaged vegetation in the Minyuan River

3.1.1 DSAL spatial zonation for vegetation survival environments

Vegetation growth primarily depends on sunshine, water, temperature and nutrients, and these inputs are directly related to environmental conditions. For example, topography influences vegetation growth in a variety of ways: elevation influences temperature, aspect determines sunshine, and slope affects hydrological conditions. In addition, the geological setting (especially lithology) controls soil properties. River basins represent natural hydrological units for which it is possible to determine balances between the major constituent fluxes of rainfall, evaporation, and river discharge, along with groundwater storage (Bathurst et al., 2010). Additionally, river basins are a natural result of changes in geomorphic processes. Hence, river basins can be characterized by their natural features, particularly in terms of topographical environments and vegetation growth.

On the basis of these natural features, the DEM and slope gradient data were mapped into four classes (1: $<\mu-\sigma$, 2: $[\mu-\sigma,\ \sigma)$, 3: $[\mu,\ \mu+\sigma]$, 4: $>\mu+\sigma$) using the mean (μ) and SD (σ) values. The slope aspect was also divided into four classes (1: [45°, 135°], 2: [135°, 225°], 3: [225°, 315°], 4: [315°, 360°] and [0°, 45°]) based on the direction of sunshine. Furthermore, lithology units in the basin can be divided into four classes of rock competence based on their lithological and structural properties (Liu et al., 2012). The classes include 1: soft rocks, Tertiary and Quaternary sediment, 2: highly fractured and weathered rocks, 3: folded, inter-bedded limestone and sandstone, 4: thickly bedded limestone, sandstone, and metamorphic rocks.

According to the above considerations, DSAL spatial zonation was defined as one spatial zonation for one given river basin, based on the natural features of the DEM, slope data, aspect data, and lithology conditions. In theory, one river basin can be mapped into 256 DSAL classes (Zhang et al., 2015).

3.1.2 Relationships between earthquake-damaged vegetation and survival environments in the Mianyuan River basin

To determine the key topographic characteristics of Mianyuan River basin, digital elevation model (DEM) data (resolution: 25 m) were extracted from a 1 : 50 000 standard topographic map (Fig. 1b) and the slope gradient and slope aspect distributions were calculated. Statistical analyses indicate that the DEM and slope gradients are normally distributed, especially for the slope gradient values, whereas slope aspects tend to be uniform. The Mianyuan River basin is primarily comprised of shale, dolomite, limestone, magmatic rocks, granite, sandstone, siltstone, and so on; all of these rocks can be divided into four classes of rock competence (Liu et al., 2012). Then, the basin was zoned spatially using the DASL zonation method (Fig. 3a). The results indicate that the basin includes 239 DSAL classes with 1994 DSAL regions; human settlements had low NDVI values and flat terrain that were extracted separately. Statistical analysis shows that similar conditions (e.g. elevation, slope gradient, slope aspect, and lithology) exist in each DSAL region.

To determine the relationships between damaged vegetation and survival environments, the vegetation damage probability (P_d) was defined as the ratio of damaged vegetation areas to total area in each of the DSAL regions. Statistical relationships between the vegetation damage probability (P_d) and the survival environments in the Mianyuan River basin are expressed via function (Eq. 3).

$$P_\mathrm{d} = \alpha D + \beta \sin(S) + \varphi\left[1 - \sin\left(\frac{A}{2}\right)\right] + \chi V, \qquad L = i \tag{1}$$

where α, β, φ, χ and i are parameters of the function 1 (Table 1), D is the ratio of the height of the contour above the base (basin mouth) to the total height of the basin, S is the slope gradient, A is the slope aspect, V is the NDVI value, and L is the code for the lithology zonation. To test the predicted values, the root mean square error (RMSE) was calculated with function (Eq. 2).

$$\mathrm{RMSE} = \sqrt{\frac{\sum_{i=1}^{n}(r_i - x_i)^2}{n}} \quad (2)$$

Here, r_i is the actual value, x_i is the predicted value, and n is the total number of samples. The result shows that the RMSE of predicted P_d is reasonable, at 0.18. In addition, to determine the recovery capacity of damaged vegetation, the vegetation recovery probability (P_r) was defined as the ratio of recovered vegetation area to total damaged vegetation area in each of the DSAL regions. Statistical relationships between the recovery probability (P_r) of damaged vegetation and the survival environments are expressed via function (Eq. 3).

$$P_\mathrm{r} = \eta D + \mu \cos(S) + \gamma \sin\left(\frac{A}{2}\right) + \tau V, \qquad L = i \quad (3)$$

Here, η, μ, γ and τ are parameters of the function 2 (Table 2). And, the RMSE of the predicted P_r was 0.37. Statistical analysis shows that most parts of the basin have high recovery probability, which is in good agreement with the actual recovered conditions (about 60.3 % of the total damaged vegetation area has recovered).

All of the above results indicate that the probabilities of vegetation damage and its recovery capacity are both strongly correlated with topographical characteristics. Additionally, these results demonstrate that DSAL spatial zonation is reasonable for detecting the relationships between earthquake-damaged vegetation and survival environments.

3.2 Relationships between vegetation and slope stability

Vegetation cover, especially of a woody type with strong and large root systems, helps to improve the stability of slopes (Gray, 1996; Wu and Sidle, 1995; Cammeraat et al.,

NHESSD
3, 3225–3250, 2015

2005; Greenwood et al., 2004). Importantly, vegetation helps to stabilize slope materials by two main mechanisms: (1) above-ground biomass changes the soil hydrology extensively through evaporation and transpiration processes (Marston, 2010; Haneberg, 1991; Harden, 2006), and leaves and litter intercept raindrops, thereby dissipating erosive energy (Parsons et al., 1996; Marston and Dolan, 1999; Keim and Skaugset, 2003), (2) the development of root systems affects the mechanical and hydrological properties of soils. Thus, vegetation improves the resistance of slopes to both surficial erosion and mass wasting. Conversely, the removal of slope vegetation tends to accelerate or increase slope failures (Gray, 1996). Although the impacts of vegetation on slope stability in mountainous regions are reasonably well understood and documented, it is still difficult to predict exactly how vegetation will impact mass movement processes including debris slides, mudflows, and rockfalls.

Endo and Tsuruta (1968) determined the reinforcement effect of a root system based on shear strength, and showed that increased strength is directly proportional to root density (Endo and Tsuruta, 1968). Roots are the primary pathway for water and nutrient uptake by plants, and the surface material along the slope creates a root ecosystem conducive to vegetation growth. The nutrient and water inputs, which control vegetation growth, are positively correlated with surface material properties. Meanwhile, surface materials make up the bulk of landslides, and landslide processes are largely determined by the slope gradient, slope materials, elevation, and hydrological conditions. All these causative factors influence vegetation growth and the vegetation survival environment. Thus, there are some coupling relationships between landslide processes and vegetation growth, and spatial analysis of landslide-damaged vegetation is important for understanding which terrain and surface materials are susceptible to landslide processes. Although there is not yet a complete understanding of the interaction of vegetation and landslide processes, these coupling relationships can be confirmed by the use of statistical analyses or other methods.

3.3 Slope stability assessment in Mianyuan River

The Wenchuan earthquake triggered many geo-hazards, especially landslides and collapses in the middle- and high-mountainous areas of China. The reduction of shear strength and overall soil cohesion, combined with ground acceleration from seismic waves, was responsible for the failure of many shallow slopes in the affected region (Yang and Chen, 2010; Zhang et al., 2012). In essence, the earthquake-induced geo-hazards are strongly controlled by the three most important factors, i.e. topographical conditions, slope material properties, and ground shaking. For it is one quite complex process that an earthquake produces a range of ground shaking levels at sites throughout the region, the ground shaking condition is more difficult to handle in modelling practice. We consider that earthquake-induced geo-hazards are much influenced by topographical conditions and slope materials properties at the basin scale.

Previous studies in the area affected by the Wenchuan earthquake have demonstrated that earthquake-induced geo-hazards are strongly correlated with elevation, slope gradient and aspect, geological units, distances to the epicenter and active faults, and seismic intensity (Huang and Li, 2009b; Qi et al., 2010; Cui et al., 2009; Dai et al., 2011; Xu et al., 2013a, b; Chen et al., 2012a, c; Zhang et al., 2011c). Our spatial distribution analysis of earthquake-damaged vegetation indicates that the probability of vegetation damage P_d is influenced by the elevation, slope gradient and aspect, lithology, and vegetative features of the slope. All of these factors can influence slope failure processes. Thus, P_d can be used as an index of slope stability susceptibility. Because function (1) is a multivariable linear regression model, the slope susceptibility (P) model in the Mianyuan River basin is expressed via function (Eq. 4).

$$P = \alpha d + \beta \sin(s) + \varphi\left[1 - \sin\left(\frac{a}{2}\right)\right] + \phi v, \quad L = i \tag{4}$$

Here, d is the ratio of the height of the contour above the base (basin mouth) to the total height of the basin, s is the slope gradient, a is the slope aspect, and v is the NDVI value. All of these variables can be obtained from thematic maps representing

NHESSD
3, 3225–3250, 2015

the various factors (e.g. elevation, slope, aspect, lithology, and NDVI). These data were used to create a map of pre-earthquake slope stability susceptibility in Mianyuan River basin (Fig. 4a).

The model results show that high-susceptibility areas were located along the steep slopes of main streams. Predicted error was defined as the difference between the mean of the values predicted by the model and the actual values in each DSAL region. The results (Fig. 4b) show good agreement between predicted susceptibility and actual conditions, except for mountaintop areas and some deep-seated landslide areas.

The above results indicate that the quantitative slope stability susceptibility should be regarded as providing a general assessment of landslide susceptibility rather than the precise probability of future landslides, owing to the complexity of the landslide processes. Actually, the predicted slope stability susceptibility at a given basin is relative, and it is no mean to compare two predicted values at different basins. In practice, it is more useful to divide the predicted slope stability susceptibility at one given basin into different levels, identifying those areas with high susceptibility to future landslides.

In addition, the recovery capacity of damaged vegetation is strongly influenced by its survival environments (especially soil moisture) (Lin et al., 2005) and the landslide processes that occurred. In the Mianyuan River basin, these unrecovered areas had suffered more serious landslide processes than the recovered areas in similar survival environments, such as the deep-seated landslides that occurred in Wenjia gully. Hence, monitoring the recovery conditions of landslide-damaged vegetation can provide useful information about the landslide processes that occurred.

4 Application

4.1 Conditions of the Subao River basin

The Subao River basin (31°44′–31°50′ N, 104°16′–104°26′ E) is located in the north-eastern part of Beichuan County, and covers an area of approximately 72.6 km^2

NHESSD
3, 3225–3250, 2015

(Fig. 5a). The main topographic features are an elevation range from 720 to 2340 m (mean elevation 1499 m) and a slope range from 0 to 75° (mean angle 30.5°). The bedrock strata in the Subao River basin range from Cambrian to Carboniferous in age, although some Quaternary deposits are distributed near the outlet of the Subao River (Zhang et al., 2011a). Rocks in this basin can be classified into eight types (Fig. 5b): dolomite and dolomitic limestone (P); siltite and quartz sandstone (S); limestone intercalated with phyllite, sandstone (LS); marlite and limestone (ML); phyllite intercalated with limestone (PL); limestone, shale, and sandstone (LSS); shale and sandstone (SS); and gravel sand and siltite (GS).

Furthermore, Subao River basin is under the influence of a humid subtropical monsoon climate, which is warm and wet. The mean annual temperature is 15.6 °C, and the mean annual precipitation is 1399 mm. As a result of this climate, the basin was well covered by forests and shrubs prior to the earthquake (Fig. 5c and d), and geo-hazards were rare (Zhang et al., 2011a). The 2008 Wenchuan earthquake struck the Subao River basin (Fig. 1a) with seismic intensity XI, and the earthquake triggered many secondary disasters (Chen et al., 2012a) such as collapses and landslides that destroyed large areas of vegetation. These earthquake-damaged vegetation areas are zonally distributed along the rivers and streams (Fig. 5e), covering an area of 11.7 km^2, which accounts for 16.1 % of the total basin area. Presently, the areas of damaged vegetation are in various stages of recovery (Fig. 5f). The analysis shows that the unrecovered areas cover approximately 3.7 km^2, which accounts for 31.5 % of the damaged area.

4.2 Assessment of slope stability susceptibility in the Subao River basin

The areas of damaged vegetation in Subao River basin were used to verify the predicted slope stability susceptibility map. To assess the accuracy of the proposed method, the predicted slope stability susceptibilities were divided into five levels and mapped (Fig. 6); the results were then compared to known landslide-prone areas, by means of high-precision imagery and field survey data (Fig. 6). Areas predicted to have high susceptibility overlapped with many of the landslide-prone areas. Statistical analysis indicated that 88.1 % of the total damaged vegetation areas have high susceptibility levels (exceeding level 3), and that 61.5 % of the total damaged vegetation areas in the Subao River basin exceeded susceptibility level 4.

In addition, the recovery conditions of damaged vegetation areas and the predicted recovery probability can be used to analyze the landslide processes that occurred during earthquake events. Statistical analysis shows that 55.4 % of the total unrecovered area has high recovery capacity (exceeding 0.60) and 11.4 % of the total recovered area has low recovery capacity (less than 0.45). These unrecovered areas with high recovery capacity had suffered more serious landslide processes than the recovered areas with low recovery capacity.

5 Discussion

We know that one key factor for earthquake-induced landslide is the grounding shaking experienced at that location during the earthquake. For example, Minayuan River is mainly located in the seismic intensity *X* zone, and the earthquake-damaged vegetation area is about 95.4 km^2 (23.2 % of the total area), while Subao River is located in the seismic intensity *XI* zone, and the earthquake-damaged vegetation area is about 11.7 km^2 (16.1 % of the total area). However, we trained the slope stability model to detect what areas are susceptible to landslides, and not to assess the actual probability of landslide occurrences during one given earthquake. Hence, we used the damaged vegetation data in Mianyuan River to train the model without considering the shaking conditions during the earthquake.

The results of the application indicate that vegetative features and data on damaged vegetation can be used to assess future landslide susceptibilities in areas recovering from an earthquake. In addition, the recovery conditions can represent the landslide processes that occurred in some conditions, and these detailed relationships require further analysis and research. Although our modeling approach would benefit from further development, the data collected to date demonstrate that this approach can be valuable for disaster mitigation efforts.

6 Conclusions

Our study presents a probabilistic approach for slope stability analysis that quantitatively relates earthquake-damaged vegetation data with slope stability susceptibilities in a given river basin. The results indicate that spatial analysis of earthquake-damaged vegetation can provide useful information about the types of terrain and surface materials that are susceptible to landslide processes, and that historical earthquake-damaged vegetation data can be used for predicting future slope instability.

Presently, the areas of damaged vegetation are in various stages of recovery and a few areas of the Wenchuan earthquake-hit area have fully recovered. In essence, these recovered areas returned to geomorphic equilibrium within a few years after the earthquake, possibly because most of the landslides that damaged vegetated areas were of shallow type, and because the high recovery capacity of the vegetation helped stabilize the slopes. Nevertheless, there remains potential for future slope instability in the region. Hence, monitoring the recovery processes of earthquake-damaged vegetated areas is helpful for understanding landslide processes and predicting future landslide hazards.

Acknowledgements. This research was financially supported by the National Science and Technology Support Program (No: 2012BAC06B02), the key Projects of the Chinese Academy of Sciences (No: KZZD-EW-05-01-04), and the Beijing Natural Science Foundation (No: 4144088).

References

Bathurst, J. C., Bovolo, C. I., and Cisneros, F.: Modelling the effect of forest cover on shallow landslides at the river basin scale, Ecol. Eng., 36, 317–327, doi:10.1016/j.ecoleng.2009.05.001, 2010.

Borgomeo, E., Hebditch, K. V., Whittaker, A. C., and Lonergan, L.: Characterising the spatial distribution, frequency and geomorphic controls on landslide occurrence, Molise, Italy, Geomorphology, 226, 148–161, doi:10.1016/j.geomorph.2014.08.004, 2014.

Cammeraat, E., van Beek, R., and Kooijman, A.: Vegetation succession and its consequences for slope stability in SE Spain, Plant Soil, 278, 135–147, 2005.

Chen, X. L., Ran, H. L., and Yang, W. T.: Evaluation of factors controlling large earthquake-induced landslides by the Wenchuan earthquake, Nat. Hazards Earth Syst. Sci., 12, 3645–3657, doi:10.5194/nhess-12-3645-2012, 2012a.

Chen, X. L., Zhou, Q., Ran, H., and Dong, R.: Earthquake-triggered landslides in southwest China, Nat. Hazards Earth Syst. Sci., 12, 351–363, doi:10.5194/nhess-12-351-2012, 2012b.

Cui, P., Chen, X., Zhu, Y., Su, F., Wei, F., Han, Y., Liu, H., and Zhuang, J.: The Wenchuan Earthquake (May 12, 2008), Sichuan Province, China, and resulting geohazards, Nat. Hazards, 56, 19–36, doi:10.1007/s11069-009-9392-1, 2009.

Cui, P., Lin, Y., and Chen, C.: Destruction of vegetation due to geo-hazards and its environmental impacts in the Wenchuan earthquake areas, Ecol. Eng., 44, 61–69, doi:10.1016/j.ecoleng.2012.03.012, 2012.

Dai, F. C., Xu, C., Yao, X., Xu, L., Tu, X. B., and Gong, Q. M.: Spatial distribution of landslides triggered by the 2008 Ms 8.0 Wenchuan earthquake, China, J. Asian Earth Sci., 40, 883–895, doi:10.1016/j.jseaes.2010.04.010, 2011.

Endo, T. and Tsuruta, T.: The effect of the tree's roots on the shear strength of soil, Annual Report, Hokkaido Branch Forest Experiment Station, Sapporo, Japan, 167–182, 1968.

Gray, D. H. and Sotir, R. B.: Biotechnical and soil bioengineering slope stabilization: a practical guide for erosion control, John Wiley and Sons, New York, 1996.

Greenwood, J., Norris, J., and Wint, J.: Assessing the contribution of vegetation to slope stability, Proc. ICE-Geotechn. Eng., 157, 199–207, 2004.

Guzzetti, F., Mondini, A. C., Cardinali, M., Fiorucci, F., Santangelo, M., and Chang, K.-T.: Landslide inventory maps: new tools for an old problem, Earth-Sci. Rev., 112, 42–66, doi:10.1016/j.earscirev.2012.02.001, 2012.

Haneberg, W. C.: Observation and analysis of pore pressure fluctuations in a thin colluvium landslide complex near Cincinnati, Ohio, Eng. Geol., 31, 159–184, 1991.
Harden, C. P.: Human impacts on headwater fluvial systems in the northern and central Andes, Geomorphology, 79, 249–263, doi:10.1016/j.geomorph.2006.06.021, 2006.
Huang, R. and Li, W.: Development and distribution of geohazards triggered by the 5.12 Wenchuan Earthquake in China, Sci. China Ser. E, 52, 810–819, doi:10.1007/s11431-009-0117-1, 2009a.
Huang, R. and Li, W.: Analysis of the geo-hazards triggered by the 12 May 2008 Wenchuan Earthquake, China, B. Eng. Geol. Environ., 68, 363–371, 2009b.
Keim, R. F. and Skaugset, A. E.: Modelling effects of forest canopies on slope stability, Hydrol. Process., 17, 1457–1467, doi:10.1002/hyp.5121, 2003.
Khan, S. F., Kamp, U., and Owen, L. A.: Documenting five years of landsliding after the 2005 Kashmir earthquake, using repeat photography, Geomorphology, 197, 45–55, doi:10.1016/j.geomorph.2013.04.033, 2013.
Koi, T., Hotta, N., Ishigaki, I., Matuzaki, N., Uchiyama, Y., and Suzuki, M.: Prolonged impact of earthquake-induced landslides on sediment yield in a mountain watershed: the Tanzawa region, Japan, Geomorphology, 101, 692–702, doi:10.1016/j.geomorph.2008.03.007, 2008.
Lee, C.-T., Huang, C.-C., Lee, J.-F., Pan, K.-L., Lin, M.-L., and Dong, J.-J.: Statistical approach to earthquake-induced landslide susceptibility, Eng. Geol., 100, 43–58, doi:10.1016/j.enggeo.2008.03.004, 2008.
Lin, W.-T., Chou, W.-C., Lin, C.-Y., Huang, P.-H., and Tsai, J.-S.: Vegetation recovery monitoring and assessment at landslides caused by earthquake in Central Taiwan, Forest Ecol. Manage., 210, 55–66, doi:10.1016/j.foreco.2005.02.026, 2005.
Liu, J. G., Mason, P. J., Yu, E., Wu, M.-C., Tang, C., Huang, R., and Liu, H.: GIS modelling of earthquake damage zones using satellite remote sensing and DEM data, Geomorphology, 139–140, 518–535, doi:10.1016/j.geomorph.2011.12.002, 2012.
Liu, Y., Liu, R., and Ge, Q.: Evaluating the vegetation destruction and recovery of Wenchuan earthquake using MODIS data, Nat. Hazards, 54, 851–862, doi:10.1007/s11069-010-9511-z, 2010.
Marston, R. A.: Geomorphology and vegetation on hillslopes: interactions, dependencies, and feedback loops, Geomorphology, 116, 206–217, 2010.

Marston, R. A. and Dolan, L. S.: Effectiveness of sediment control structures relative to spatial patterns of upland soil loss in an arid watershed, Wyoming, Geomorphology, 31, 313–323, doi:10.1016/S0169-555X(99)00089-6, 1999.

Parsons, A. J., Abrahams, A. D., and Wainwright, J.: Responses of interrill runoff and erosion rates to vegetation change in southern Arizona, Geomorphology, 14, 311–317, 1996.

Peruccacci, S., Brunetti, M. T., Luciani, S., Vennari, C., and Guzzetti, F.: Lithological and seasonal control on rainfall thresholds for the possible initiation of landslides in central Italy, Geomorphology, 139, 79–90, 2012.

Qi, S., Xu, Q., Lan, H., Zhang, B., and Liu, J.: Spatial distribution analysis of landslides triggered by 2008.5.12 Wenchuan Earthquake, China, Eng. Geol., 116, 95–108, doi:10.1016/j.enggeo.2010.07.011, 2010.

Tang, C., Zhu, J., Qi, X., and Ding, J.: Landslides induced by the Wenchuan earthquake and the subsequent strong rainfall event: a case study in the Beichuan area of China, Eng. Geol., 122, 22–33, doi:10.1016/j.enggeo.2011.03.013, 2011.

Wu, W. and Sidle, R. C.: A distributed slope stability model for steep forested basins, Water Resour. Res., 31, 2097–2110, 1995.

Xu, C., Xu, X., Yao, Q., and Wang, Y.: GIS-based bivariate statistical modelling for earthquake-triggered landslides susceptibility mapping related to the 2008 Wenchuan earthquake, China, Quarterly J. Eng. Geol. Hydrogeol., 46, 221–236, 2013a.

Xu, C., Xu, X., Yao, X., and Dai, F.: Three (nearly) complete inventories of landslides triggered by the May 12, 2008 Wenchuan Mw 7.9 earthquake of China and their spatial distribution statistical analysis, Landslides, 11, 441–461, doi:10.1007/s10346-013-0404-6, 2013b.

Yang, X. and Chen, L.: Using multi-temporal remote sensor imagery to detect earthquake-triggered landslides, Int. J. Appl. Earth Observ. Geoinf., 12, 487–495, doi:10.1016/j.jag.2010.05.006, 2010.

Zhang, H., Chi, T., Fan, J., Hu, K., and Peng, L.: Spatial Analysis of Wenchuan Earthquake-Damaged Vegetation in the Mountainous Basins and Its Applications, Remote Sensing, 7, 5785–5804, 2015.

Zhang, J., Cui, P., Ge, Y., and Xiang, L.: Susceptibility and risk assessment of earthquake-induced landslides based on Landslide Response Units in the Subao River basin, China, Environ. Earth Sci., 65, 1037–1047, doi:10.1007/s12665-011-1002-3, 2011.

Zhang, J., Hull, V., Huang, J., Yang, W., Zhou, S., Xu, W., Huang, Y., Ouyang, Z., Zhang, H., and Liu, J.: Natural recovery and restoration in giant panda habitat after the Wenchuan earthquake, Forest Ecol. Manage., 319, 1–9, doi:10.1016/j.foreco.2014.01.029, 2014.

Zhang, L. M., Xu, Y., Huang, R. Q., and Chang, D. S.: Particle flow and segregation in a giant landslide event triggered by the 2008 Wenchuan earthquake, Sichuan, China, Nat. Hazards Earth Syst. Sci., 11, 1153–1162, doi:10.5194/nhess-11-1153-2011, 2011.

Zhang, S., Zhang, L. M., Peng, M., Zhang, L. L., Zhao, H. F., and Chen, H. X.: Assessment of risks of loose landslide deposits formed by the 2008 Wenchuan earthquake, Nat. Hazards Earth Syst. Sci., 12, 1381–1392, doi:10.5194/nhess-12-1381-2012, 2012.

Table 1. Parameters of the function (Eq. 1) in the Mianyuan River basins.

Lithology ($L = i$)	α	β	φ	χ	R^2
$L = 1$	−0.040	1.086	0.251	−0.793	0.706
$L = 2$	0.169	0.909	−0.235	−0.613	0.680
$L = 3$	−0.236	1.123	0.127	−0.614	0.823
$L = 4$	−0.398	1.222	0.233	−0.492	0.812

NHESSD
3, 3225–3250, 2015

Table 2. Parameters of the function (Eq. 3) in the Mianyuan River basins.

Lithology ($L = i$)	η	μ	γ	τ	R^2
$L = 1$	0.331	−0.037	0.586	0.150	0.716
$L = 2$	−0.369	1.142	−0.135	0.021	0.683
$L = 3$	0.387	0.141	0.021	0.824	0.603
$L = 4$	−0.879	0.637	0.122	0.580	0.702

NHESSD

3, 3225–3250, 2015

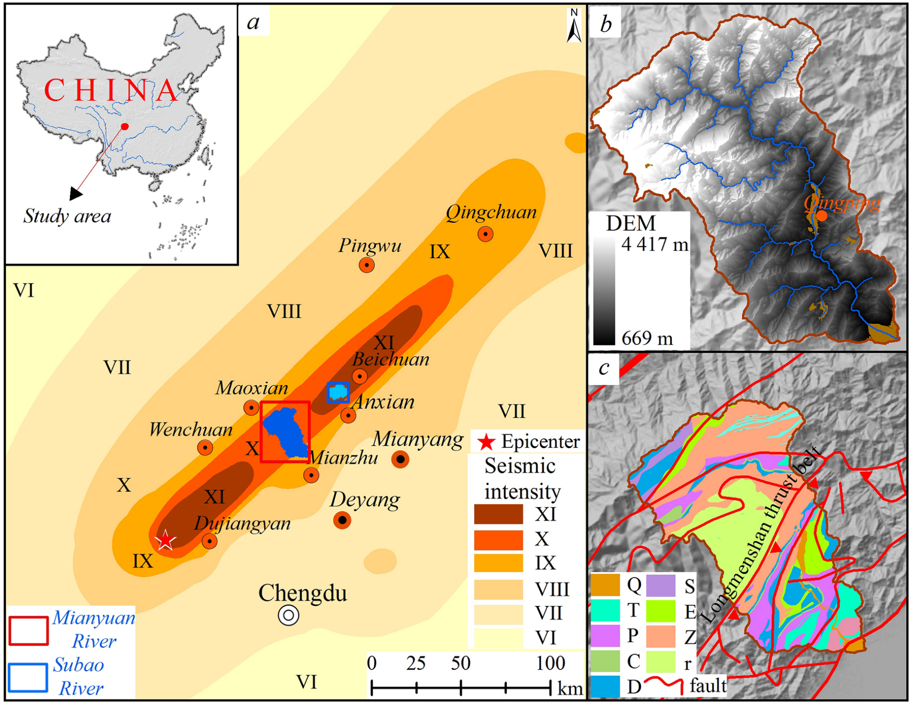

Figure 1. The study area: **(a)** Seismic intensity map and Mianyuan River location. **(b)** Digital elevation model (DEM) map of Mianyuan River. **(c)** Simplified geological map of Mianyuan River.

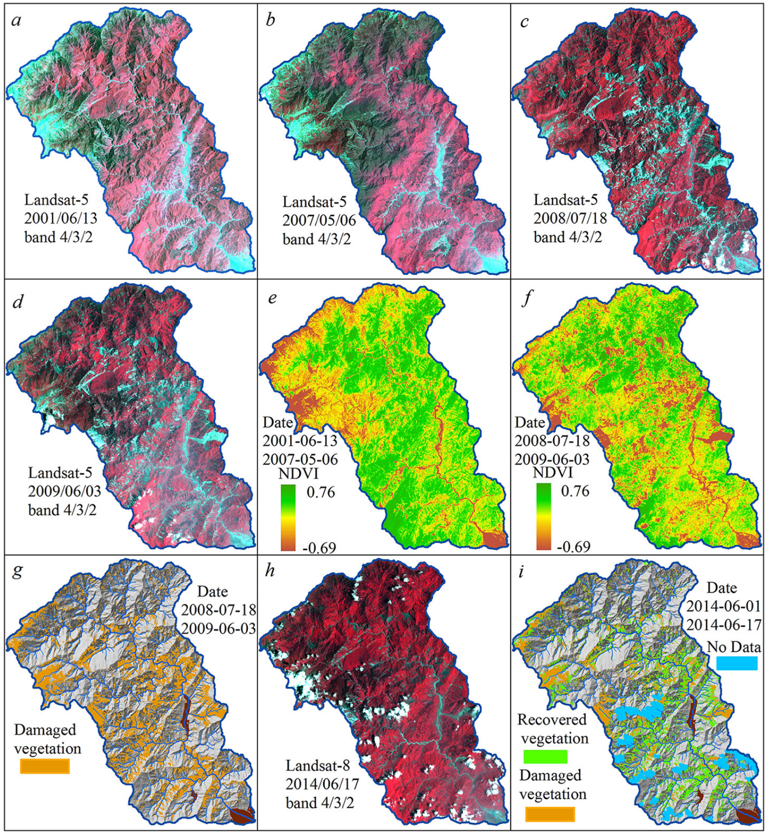

Figure 2. 2001–2014 vegetation changes in Mianyuan River basin: **(a)** 13 June 2001 TM image. **(b)** 06 May 2007 TM image. **(c)** 18 July 2008 TM image. **(d)** 3 June 2009 TM image. **(e)** Pre-earthquake NDVI image. **(f)** Post-earthquake NDVI image. **(g)** Earthquake-damaged vegetation map. **(h)** 17 June 2014 Landsat-8 images. **(i)** Recovered vegetation (until 17 June 2014) map.

NHESSD
3, 3225–3250, 2015

NHESSD
3, 3225–3250, 2015

Spatial analysis of damaged vegetation in the Mianyuan River basin

H. Z. Zhang et al.

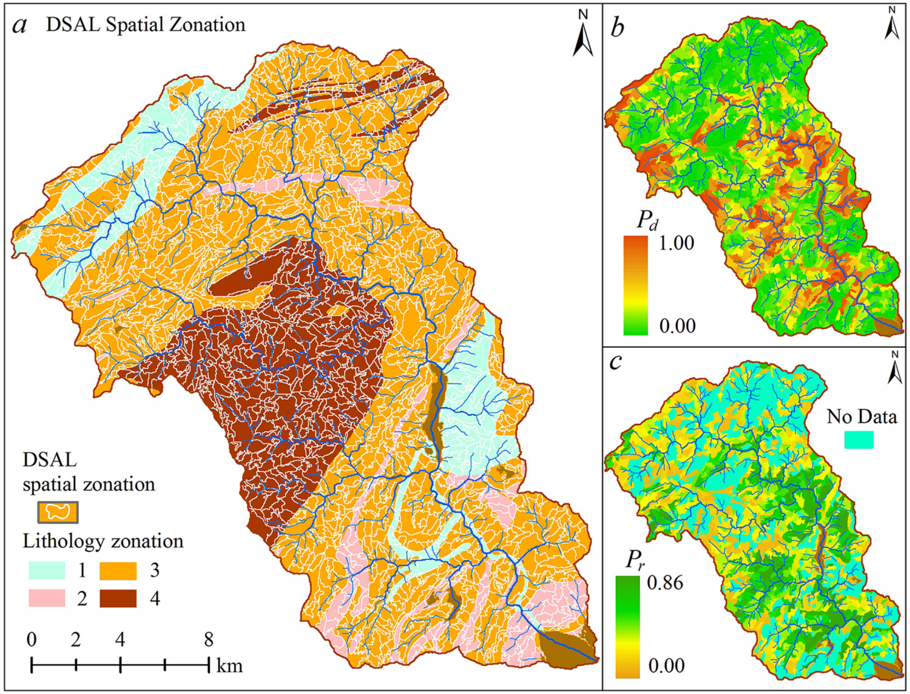

Figure 3. (a) DSAL (digital elevation model, slope, aspect, and lithology) spatial zonation map of Mianyuan River basin. **(b)** Vegetation damage probability P_d in each zonation. **(c)** Vegetation recovery probability P_r in each zonation.

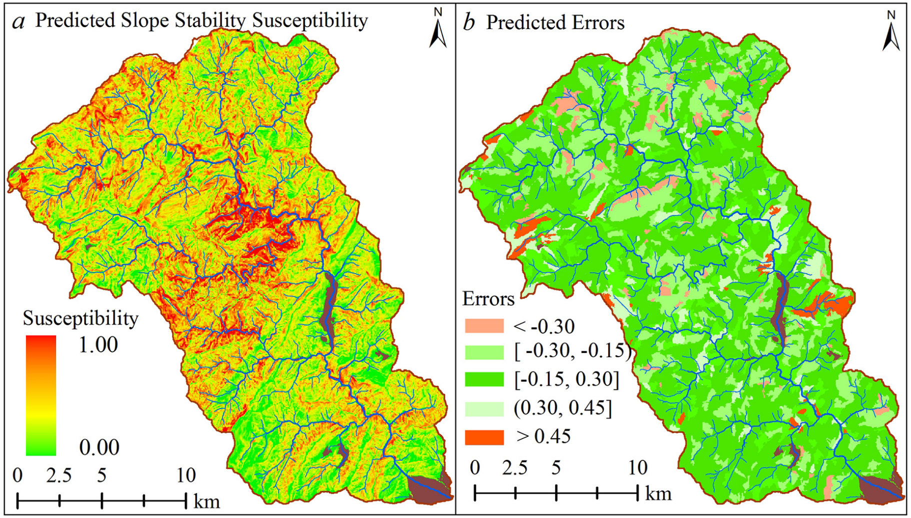

Figure 4. Predicted slope susceptibility in Mianyuan River basin **(a)** and distribution of prediction error **(b)**.

NHESSD
3, 3225–3250, 2015

Title Page
Abstract
Introduction
Conclusions
References
Tables
Figures
◂
▸
Back
Close
Full Screen / Esc
Printer-friendly Version
Interactive Discussion

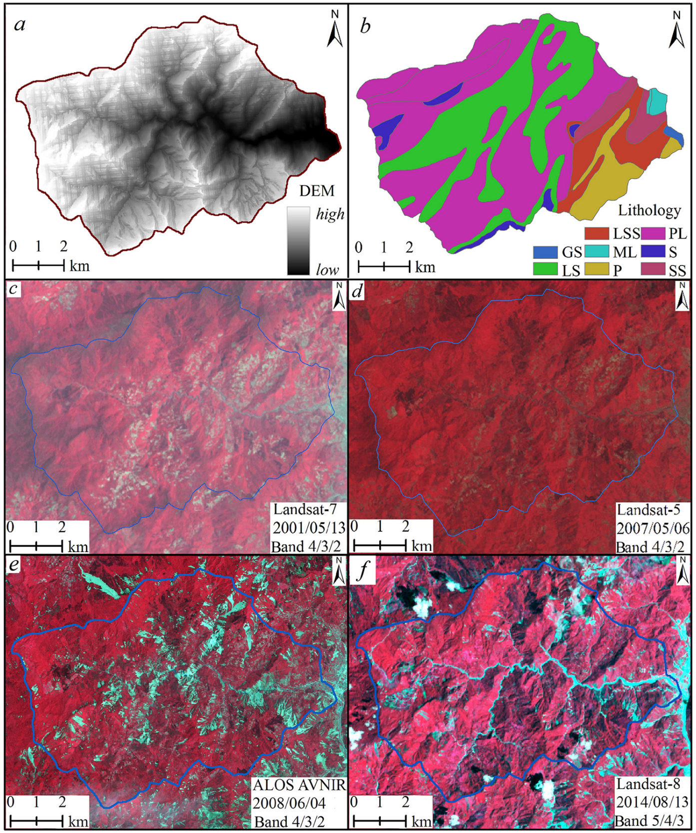

Figure 5. Subao River basin: **(a)** digital elevation model (DEM). **(b)** Lithology image. **(c)** 13 May 2001 Landsat-7 image. **(d)** 6 May 2007 Landsat-5 image. **(e)** 4 June 2008 ALOS image. **(f)** 13 August 2014 Landsat-8 image.

NHESSD
3, 3225–3250, 2015

Spatial analysis of damaged vegetation in the Mianyuan River basin

H. Z. Zhang et al.

Title Page
Abstract | Introduction
Conclusions | References
Tables | Figures
◄ | ►
◄ | ►
Back | Close
Full Screen / Esc
Printer-friendly Version
Interactive Discussion

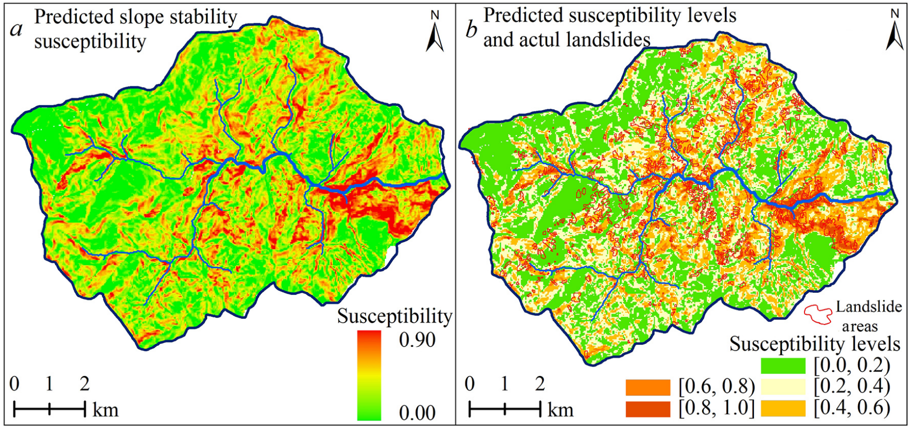

Figure 6. Predicted slope stability **(a)** and the susceptibility levels **(b)** in the Subao River basin.